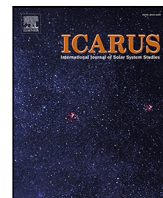




<b>Publication Year</b>	2024
<b>Acceptance in OA</b>	2024-12-11T11:10:17Z
<b>Title</b>	Experimental study on the radiation-induced destruction of organic compounds on the surface of the Moon
<b>Authors</b>	Dalla Pria, G.L., Sohler, O., SCIRE' SCAPPUZZO, Carlotta, URSO, Riccardo Giovanni, BARATTA, Giuseppe, PALUMBO, Maria Elisabetta
<b>Publisher's version (DOI)</b>	10.1016/j.icarus.2024.116077
<b>Handle</b>	<a href="http://hdl.handle.net/20.500.12386/35452">http://hdl.handle.net/20.500.12386/35452</a>
<b>Journal</b>	ICARUS
<b>Volume</b>	415



# Experimental study on the radiation-induced destruction of organic compounds on the surface of the Moon

G.L. Dalla Pria<sup>a,b</sup>, O. Sohier<sup>a,c,1</sup>, C. Scirè<sup>a</sup>, R.G. Urso<sup>a</sup>, G.A. Baratta<sup>a</sup>, M.E. Palumbo<sup>a,\*</sup>

<sup>a</sup> INAF-Osservatorio Astrofisico di Catania, Via Santa Sofia 78, Catania, 95123, Italy

<sup>b</sup> Luleå University of Technology, Laboratorievägen 14, Luleå, 97187, Sweden

<sup>c</sup> Université de Versailles Saint-Quentin-en-Yvelines, 55 avenue de Paris, Versailles, 78035, France

## ARTICLE INFO

### Keywords:

Astrobiology  
Astrochemistry  
Ice spectroscopy  
Laboratory astrophysics  
Lunar surface

## ABSTRACT

Volatile organic molecules and a complex organic refractory material were detected on the Moon and on lunar samples. The Moon's surface is exposed to a continuous flux of solar UV photons and fast ions, e.g. galactic cosmic rays (GCRs), solar wind (SW), and solar energetic particles (SEPs), that modify the physical and chemical properties of surface materials, thus challenging the survival of organic compounds. With this in mind, the aim of this work is to estimate the lifetime of organic compounds on the Moon's surface under processing by energetic particles. We performed laboratory experiments to measure the destruction cross section of selected organic compounds, namely methane (CH<sub>4</sub>), formamide (NH<sub>2</sub>CHO), and an organic refractory residue, under simulated Moon conditions. Volatile species were deposited at low temperature (17 - 18 K) and irradiated with energetic ions (200 keV) in an ultra-high vacuum chamber. The organic refractory residue was produced after warming up of a CO:CH<sub>4</sub> ice mixture irradiated with 200 keV H<sup>+</sup> at 18 K. All the samples were analyzed in situ by infrared transmission spectroscopy. We found that destruction cross sections are strongly affected (up to one order of magnitude) by the dilution of a given organic in an inert matrix. Among the selected samples, organic refractory residues are the most resistant to radiation. We estimated the lifetime of organic compounds on the surface of the Moon by calculating the dose rate due to GCRs and SEPs at the Moon's orbit and by using the experimental cross section values. Taking into account impact gardening, we also estimated the fraction of surviving organic material as a function of depth. Our results are compatible with the detection of CH<sub>4</sub> in the LCROSS eject plume originating from layers deeper than about 0.7 m at the Moon's South Pole and with the identification of complex organic material in lunar samples collected by Apollo 17 mission.

## 1. Introduction

Between 1969 and 1972, Apollo missions brought back 382 kg of rocks from the lunar surface; H<sub>2</sub>O and other volatile species have been the subject of intense study because they offer important constraints on the Moon's origin and evolution, as well as for evaluating potential future human exploration (e.g. Jones et al., 2020, 2021; McLain et al., 2021; Clendenen et al., 2022). Whether significant amounts of organic compounds were present was one of the most carefully researched questions following the gathering of Apollo lunar samples. Interest in the nature of lunar organic matter has continued to the present day, with indigenous complex organic material recently identified for the first time in Apollo 17 samples. Indeed, Thomas-Keppta et al. (2014) has revealed that non-terrestrial, complex organic matter is intimately associated with glass beads collected during the mission. C-rich micrometeorites and interplanetary dust particles (IDPs) are described

as contributors to the abiotic organic inventory of the early Earth and possibly of the lunar regolith. Any material placed or exposed on the surface of bodies without a substantial atmosphere and a global magnetic field is subject to weathering by galactic cosmic rays (GCRs), solar wind (SW), and solar energetic particles (SEPs) (e.g. Glotch et al., 2019). Crites et al. (2013) showed that GCR protons provide enough energy to stimulate chemistry over the time available for ices to be retained in lunar cold traps (1–2 Ga); on the one hand, dose rate calculations indicate that organic synthesis is plausible well within the age of the lunar polar cold traps and that organics detected at the poles of the Moon may have been produced in situ. On the other hand, several laboratory investigations showed that organic matter can be destroyed by exposure to energetic ions (e.g. Gerakines et al., 2012; Gerakines and Hudson, 2013; De Sanctis et al., 2023). In light of this, the focus of this paper is on the survival of organic compounds to energetic ions on

\* Corresponding author.

E-mail addresses: [gaidal-3@student.ltu.se](mailto:gaidal-3@student.ltu.se) (G.L. Dalla Pria), [maria.palumbo@inaf.it](mailto:maria.palumbo@inaf.it) (M.E. Palumbo).

<sup>1</sup> LATMOS/IPSL, UVSQ Université Paris-Saclay, Sorbonne Université, CNRS, Guyancourt, France.

the Moon's surface. For our study, we have selected some representative organic samples, namely methane ( $\text{CH}_4$ ), formamide ( $\text{NH}_2\text{CHO}$ ) and an organic refractory residue. Many factors have influenced the choice of chemicals to employ:  $\text{CH}_4$  is the simplest hydrocarbon and a widely spread molecule along the line of sight to star forming regions (e.g. Cruikshank et al., 2000; Grundy and Buie, 2001; Fulvio et al., 2010; Boogert et al., 2015; Barucci and Merlin, 2020). In addition, proof of the presence of  $\text{CH}_4$  was found on the Moon, during LCROSS mission when the lunar south pole crater Cabeus was impacted by a spent Centaur rocket which caused debris, dust, and vapor to be ejected (Colaprete et al., 2010); from spectral fits, the authors derived a relative abundance of 0.65% for  $\text{CH}_4$  w.r.t. to  $\text{H}_2\text{O}$ .

Formamide ( $\text{NH}_2\text{CHO}$ ) is a molecule that belongs to the amide family and includes a peptide bond. Several studies showed that it can act as a precursor in the formation of amino and nucleic acids (Saladino et al., 2005, 2009, 2012; Pino et al., 2015), making it one of the possible players in pre-biotic chemistry.  $\text{NH}_2\text{CHO}$  has been observed in cometary comae and on the comet 67P/C-G during the Rosetta mission (Bockelée-Morvan et al., 2000; Goesmann et al., 2015). In particular, Goesmann et al. (2015) reported that the abundance of this molecule can be as high as 1.8% w.r.t. water. Furthermore, Schutte et al. (1999) and Raunier et al. (2004) reported a tentative detection of solid formamide in the line-of-sight of young stellar objects observed with the Infrared Space Observatory-Short Wavelength Spectrometer (ISO-SWS).

An organic refractory residue is an organic-rich material left over after irradiation of simple ices containing C-bearing species (e.g. Palumbo et al., 2004; Baratta et al., 2015; Accolla et al., 2018; Baratta et al., 2019). Analysis by infrared spectroscopy and mass spectrometry indicate that organic refractory residues contains thousands of organic compounds, including species of relevance for Astrobiology, such as amino acids, sugars, and nucleobases (e.g. Danger et al., 2013; Meinert et al., 2016; Materese et al., 2017; Accolla et al., 2018; Nuevo et al., 2018; Urso et al., 2020). As discussed by Baratta et al. (2019) organic refractory residues obtained after ion irradiation of simple ices can be considered analogues of organic matter in space. Indeed residues produced in laboratory from ion irradiation of simple ice mixtures are good spectral analogue of extraterrestrial organic material detected in micrometeorites and interplanetary dust particles (IDPs) (Baratta et al., 2015; Potapov et al., 2022).

The aim of our experimental investigations is to consider different ice mixtures or organic refractory samples in order to constrain the range of destruction cross section values of relevant compounds. In the experiments here presented,  $\text{CH}_4$  is mixed with  $\text{N}_2$ . The idea is to mix  $\text{CH}_4$  in an H-poor matrix to reduce as many backward reactions as possible; these would, indeed, reform  $\text{CH}_4$ . On the other hand additional destruction pathways which include  $N$  could take place to better simulate the presence of  $\text{CH}_4$  in trace amounts. Similarly, we investigated the case of an organic-rich environment (pure  $\text{NH}_2\text{CHO}$ ) and the case of  $\text{NH}_2\text{CHO}$  diluted in an inert matrix. These extreme cases, none of which is realistic, allow us to measure the upper and lower limit of the destruction cross section. Furthermore,  $\text{N}_2:\text{CH}_4$  mixtures and the organic residues are irradiated with different ions, namely  $\text{H}^+$ ,  $\text{He}^+$ , and  $\text{N}^+$ , at 200 keV to take into account the most abundant species in SEPs and to investigate any difference due to the impinging projectile.

The manuscript is organized as follows: in Section 2 the experimental set-up and procedures are described, in Section 3 the experimental results are presented and their relevance is discussed in Section 4.

## 2. Materials and methods

The experiments presented here have been conducted in the Laboratory for Experimental Astrophysics (LASp) at INAF - Osservatorio Astrofisico di Catania (Italy). All the experiments are performed in an ultra-high vacuum (UHV) chamber ( $P < 10^{-9}$  mbar), shown in Fig. 1. Ice samples are accreted on an infrared transparent substrate

(KBr) placed in thermal contact with the final tail (cold finger) of a closed-cycle helium Cryocooler (CTI) that allows temperatures to vary between 17 and 300 K. Gas phase species, except than formamide, are admitted in the UHV chamber through the main gas inlet shown in Fig. 1. A dedicated mixing chamber is used to prepare the gaseous mixture and to admit it into the UHV chamber by means of a needle valve, resulting in a background deposition of ice onto the substrate. This method has the advantage that the film deposited has a uniform thickness, but has the disadvantage that gas phase molecules can freeze out onto all cold surfaces inside the chamber. To prevent any deposition on the backside of the substrate, this is protected by a copper tube aligned with the IR beam and with the central hole of the cold finger (Scirè et al., 2019). During deposition the thickness of the ice sample is monitored by looking at the interference pattern produced by a He-Ne laser beam reflected at near normal incidence by the vacuum-film and film-substrate interfaces. Laser light enters and leaves the chamber through a fused silica window (labeled "multipurpose window" in Fig. 1) whose surface is parallel to the substrate inside the chamber (Urso et al., 2016; Scirè, 2017). The trend of the interference curve confirms that the deposition rate is constant during accretion and, hence that, the composition of the mixture is homogeneous in the ice sample. Due to its low vapor pressure, formamide was admitted in the UHV chamber through an inlet mounted on the multipurpose window. In this case, the thickness of the sample is obtained thanks to calibration experiments previously performed (see e.g. Brucato et al., 2006). The UHV chamber is directly connected to a 200 kV ion implanter (Danfysik 1080-200). The ion beam is electrostatically swept to ensure a uniform coverage on the target. In order to avoid a macroscopic heating of the sample, the ion current density is maintained between  $100 \text{ nA cm}^{-2}$  and a few  $\mu\text{A cm}^{-2}$ . The ion fluence (ions  $\text{cm}^{-2}$ ) is measured by integrating the ion current monitored during irradiation. After deposition, the ice mixtures are irradiated with 200 keV ions (namely  $\text{H}^+$ ,  $\text{He}^+$  or  $\text{N}^+$ ). The energy deposited by incoming ions to the sample (dose,  $\text{eV}/16\text{u}$ ) is calculated by multiplying the fluence measured during irradiation and the stopping power ( $\text{eV cm}^{-2}$  per molecule) given by the SRIM software (Ziegler, 1977; Ziegler et al., 1996). The thickness of the samples is kept lower than the penetration depth of impinging ions in order to have a rather uniform energy loss of the ions over the thickness of the ice layer. All the samples are analyzed in situ by a Fourier Transform Infrared (FTIR) spectrometer (Bruker, Vertex 70). Spectra with a resolution of  $1 \text{ cm}^{-1}$  and sampling of  $0.25 \text{ cm}^{-1}$  are taken. The substrate forms an angle of  $45^\circ$  both with the ion beam and with the infrared beam coming from the IR source of the spectrometer. A hole in the cold finger allows the infrared beam to be transmitted through the infrared transparent substrate so that transmittance IR spectra can be easily taken in situ, even during ion bombardment, without tilting the sample. A rotatable polarizer placed along the path of the IR beam allows to take spectra both with the electric vector parallel (P-polarized) and perpendicular (S-polarized) to the plane of incidence of the infrared beam. In this work, all the shown spectra are acquired in P-polarization because of a better signal-to-noise ratio; indeed, the transmitted signal in P-polarization is higher than the transmitted signal in S-polarization (e.g. Brucato et al., 2006; Urso et al., 2017).

### 2.1. Ice mixtures

Three  $\text{N}_2:\text{CH}_4 = 1:1$  mixtures are deposited on KBr substrates at 17 K and exposed to 200 keV  $\text{H}^+$ ,  $\text{He}^+$  and  $\text{N}^+$ , respectively. Pure formamide and a  $\text{Ar}:\text{NH}_2\text{CHO} = 25:1$  mixture are accreted onto the cold KrB substrate at 17.5 K. After deposition,  $\text{NH}_2\text{CHO}$  and the  $\text{Ar}:\text{NH}_2\text{CHO}$  mixture were irradiated with 200 keV  $\text{H}^+$ . In all cases IR transmittance spectra are taken at several intermediate steps of irradiation. It is known that, among others, ion irradiation causes a removal of surface molecules. This effect, known as sputtering, depends on the mass and energy of impinging ions (e.g. Rothard et al., 2017). While sputtering

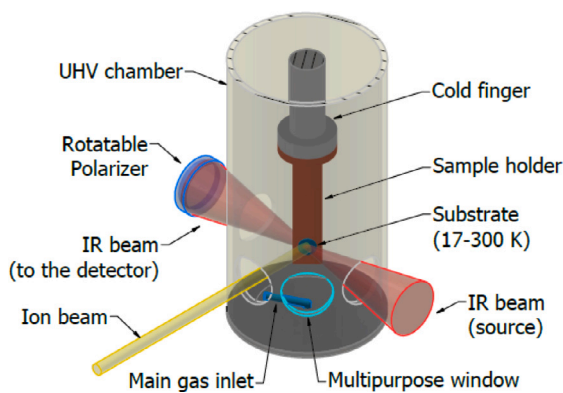


Fig. 1. Schematic view of the experimental set-up.

is negligible after ion irradiation with 200 keV protons (e.g. Loeffler et al., 2005), it is very relevant after irradiation with heavy ions (e.g. Seperuelo Duarte et al., 2010). In order to quantitatively study the destruction of original species induced by ion irradiation it is important to disentangle the effects of sputtering occurring at the surface from the chemical effects occurring in the bulk. With this in mind, prior to irradiation a 300 nm layer of Ar was deposited on each  $N_2:CH_4$  sample. The Ar layer was thick enough to avoid that sputtering affected the  $N_2:CH_4$  sample after irradiation with 200 keV  $He^+$  and  $N^+$  ions. The Ar layer was not deposited on the  $NH_2CHO$  and  $Ar:NH_2CHO$  samples that were irradiated only with 200 keV  $H^+$  ions.

Ice mixtures were selected to constrain the range of destruction cross section values of relevant compounds.  $N_2:CH_4$  mixtures are selected as a template of a sample where we do not expect backward reactions (C+H) but we have additional destruction pathways which include N. In the case of formamide, we considered two extreme cases, pure formamide and formamide diluted in Ar, in order to analyze the upper and lower limits of the destruction cross section range.

## 2.2. Organic refractory residue

A  $CO:CH_4 = 1:1$  ice mixture (about 1.2  $\mu m$  thick) is bombarded by 200 keV  $H^+$  ions at 18 K up to a dose of 120 eV/16u and subsequently warmed up to room temperature to form the organic refractory residue, as shown by Palumbo et al. (2004) and Accolla et al. (2018). Earlier measurements by Baratta et al. (2015) show that the thickness of the residue typically decreases by 85%–90% compared to the thickness of the un-irradiated ice. Here the thickness of the residue should be in the range of 0.12–0.18  $\mu m$ . The residue is then irradiated at 200 K by 200 keV ions; three organic refractory residues are produced and irradiated with  $H^+$ ,  $He^+$ , and  $N^+$  ions, respectively. IR spectra of several organic refractory residues are shown by Accolla et al. (2018). The absorption bands present in the spectra of the residue depend on the molecules selected for the initial ice mixtures. If a nitrogen bearing species is present (e.g.  $N_2$ ) N-H, and C-N vibrational modes are observed in the spectrum of the residue. Since the N-H stretching mode partially overlaps with the C-H stretching mode, in the present study we formed the residue starting with a  $CO:CH_4$  ice mixture (i.e. without any N-bearing species). In this case it is possible to obtain the C-H destruction cross section with higher confidence.

In our experimental conditions, the organic refractory residue is stable at room temperature (Baratta et al., 2019) while  $N_2:CH_4$  ice mixtures sublimates at about 30 K (e.g. Collings et al., 2004) and pure formamide at about 160 K (e.g. Urso et al., 2017). In astrophysical environments, ices are expected to be present in cold regions while refractory organic material can be present both in cold regions and in warm regions. The temperature of the surface of the Moon at the

equator varies between 400 K (daytime) and 140 K (at night) while at the poles can be as low as 20 K. In this work organic refractory residues have been irradiated at 200 K considering this value as an average value for the temperature of organic refractory matter on the lunar surface.

## 2.3. OMERE and SRIM software

We used the software Outil de Modélisation de l'Environnement Radiatif Externe (OMERE) to evaluate the effects of GCRs and SEPs on the Moon. OMERE is a freeware developed by TRAD with support from CNES, (<https://www.trad.fr/spatial/logiciel-omere/>). OMERE computes the space environment in terms of particle fluxes and, for a given material, the dose rate ( $rad\ a^{-1}$ ) as a function of depth. The calculations can be performed on available orbits or using orbital parameters introduced by the user.

Since OMERE does not account for particles with energy below 10 keV, we estimate the effects of SW ions by means of the software The Stopping and Range of Ions in Matter (SRIM, <http://www.srim.org/>). It is a group of programs which calculate the stopping and range of ions into matter using a quantum mechanical treatment of ion-atom collisions (Ziegler, 1977; Ziegler et al., 1996).

The penetration depth of energetic ions depends on its mass and initial energy. For a given ion mass the higher is the initial energy the higher is the penetration depth (that is the depth traveled before stopping). As an example, 10 MeV protons would travel in  $SiO_2$  longer than 1 keV protons. SRIM simulations show that  $H^+$  and  $He^+$  ions with energy 1–4 keV do not penetrate deeper than about 0.1  $\mu m$ , while 10 MeV protons penetrate about 600  $\mu m$ .

## 3. Results

### 3.1. $N_2:CH_4$ ice mixtures

In Fig. 2 the IR spectra of a  $N_2:CH_4$  ice mixture irradiated at 17 K with 200 keV  $He^+$  ions are shown in the spectral range of methane C-H stretching ( $3012\ cm^{-1}$ ) and bending ( $1301\ cm^{-1}$ ) peaks. The related normalized band area values as a function of the irradiation dose are reported in Fig. 3. The experimental data are fitted by the exponential curve

$$y = Ae^{-\sigma D} + y_0, \quad (1)$$

where  $D$  is the dose (eV/16u),  $\sigma$  is the cross section (16u/eV),  $y_0$  is the asymptotic value and  $A + y_0 = 1$ . The cross sections values obtained by the fit are reported in Table 1. The fit results are really good with all the coefficients of correlation above 0.99. The good quality of the exponential fit indicates that the destruction of original molecules after ion irradiation is a first order process. Fig. 3 shows that the band area rapidly decreases at the beginning of irradiation and then reaches a saturation value. We notice that the initial decrease follows the same trend for the three experiments while the saturation value is about 0.1 in the case of irradiation with 200 keV  $H^+$  and  $He^+$  ions, and it is about 0.2 in the case of irradiation with 200 keV  $N^+$  ions. We speculate that this difference is due to the lower penetration depth of  $N^+$  ions in the target ice, as estimated by means of SRIM software (Ziegler et al., 1996). In fact in the passage through a solid target energetic ions lose energy both to electronic excitations and to momentum transfer to target nuclei (e.g. Johnson, 1990; Rothard et al., 2017). As a consequence the energy loss per unit path length, often referred to as stopping power, determines the penetration depth of impinging ions. In turns, at a given energy, ions with higher stopping power values travel a shorter distance in matter. As given by SRIM software (Ziegler et al., 1996) the stopping power of  $N^+$  ions in a  $N_2:CH_4$  ice sample is about 26 eV/Å that is higher than the stopping power of  $H^+$  and  $He^+$  ions, about 6.5 eV/Å and 16 eV/Å respectively. Similar values of cross sections, under the irradiation with the three different ions, are found. It can be concluded that the destruction cross section of C-H bonds in  $N_2:CH_4$  ice mixture does not depend on the ions that irradiate the material.

**Table 1**  
Comparison of cross sections. The organic materials are listed from the most volatile to the most refractory.

Organic material	Temperature (K)	Ion type	Cross section (16u/eV)
$N_2:CH_4$	17	$H^+$	$0.077 \pm 0.007$
		$He^+$	$0.079 \pm 0.006$
		$N^+$	$0.077 \pm 0.004$
$NH_2CHO$	17.5	$H^+$	$0.055 \pm 0.003$
		$He^+$	$0.061 \pm 0.002$
		$N^+$	$0.063 \pm 0.002$
$Ar:NH_2CHO=25:1$	17.5	$H^+$	$0.045 \pm 0.004$
		$He^+$	$0.886 \pm 0.143$
Organic refractory residue	200	$H^+$	$0.002 \pm 0.0003$
		$He^+$	$0.008 \pm 0.0006$
		$N^+$	$0.024 \pm 0.002$

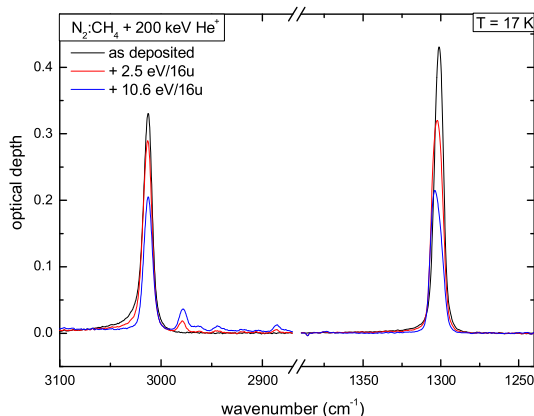


**Fig. 2.** Evolution of C-H stretching and bending peaks for  $N_2:CH_4$  mixture after ion irradiation: the initial stage is represented in black, and two steps of irradiation in red and blue. (For interpretation of the references to color in this figure legend, the reader is referred to the web version of this article.)

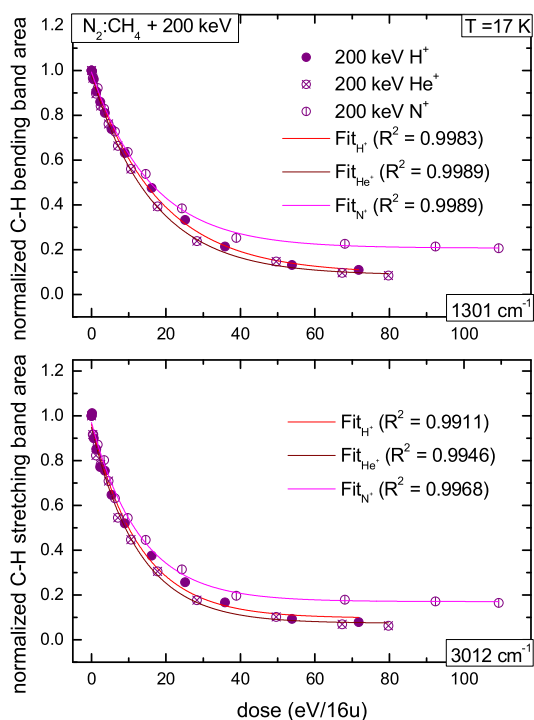


**Fig. 3.** Normalized C-H bending and C-H stretching band area of  $N_2:CH_4$  mixtures after ion bombardment plotted vs. irradiation dose. The graphs show data resulting from the irradiation with  $H^+$ ,  $He^+$  and  $N^+$  200 keV ions and the fit obtained using Eq. (1).

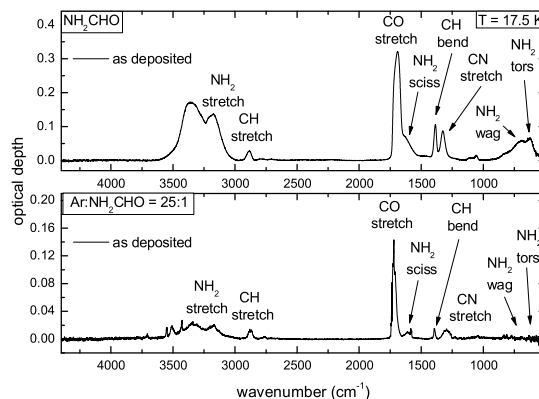


**Fig. 4.** Infrared spectra in optical depth scale of pure and diluted formamide (17.5 K) samples acquired before irradiation with 200 keV  $H^+$  ions.

### 3.2. Pure and diluted $NH_2CHO$

In Fig. 4 the IR spectra of pure  $NH_2CHO$  and a  $Ar:NH_2CHO = 25:1$  mixture are shown; following Brucato et al. (2006) and Urso et al. (2017), the main vibrational features are labeled. The profile of the infrared bands shows significant differences: in general, formamide diluted in an Ar matrix has narrower bands. A similar result is obtained for a  $CO:NH_2CHO$  mixture (e.g. Urso et al., 2017). In Fig. 5 there is a detail of the spectra in the C-H bending ( $1388\text{ cm}^{-1}$ ) and C-N stretching ( $1328\text{ cm}^{-1}$ ) peak regions: the initial (black line) and two steps (red and blue lines) of irradiation are reported. In Fig. 6 the values of the normalized band area for the two ice samples are plotted. In the case of pure formamide, we considered the area of the double peak feature due to the superposition of the C-H bending and C-N stretching modes; instead, for  $Ar:NH_2CHO$  mixture, the area of the C-H bending mode band was evaluated. Experimental data are fitted with an exponential equation (Eq. (1)). The fit gives the cross section values ( $\sigma$ ) reported in Table 1. The normalized band area is the area of the band at each step of irradiation divided by the initial value before irradiation. We notice that after the first step of irradiation the area of the band increases and the normalized value is greater than 1. This effect has been observed also after ion irradiation of other ice samples (e.g. Loeffler et al., 2005; Garozzo et al., 2011) and is ascribed to a modification of the structure of the sample which in turn causes a variation of the band strength value.

### 3.3. Organic refractory residue

In Fig. 7, the IR spectra of an organic refractory residue in the  $3150\text{--}2650\text{ cm}^{-1}$  region are shown; the three peaks close to each other ( $2960$ ,  $2927$  and  $2870\text{ cm}^{-1}$ ) are characteristic of the aliphatic  $-CH_2$  and  $-CH_3$  bonds. Three samples have been irradiated with 200 keV  $H^+$ ,

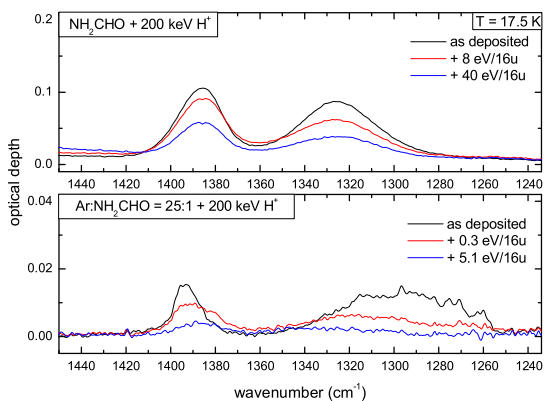


**Fig. 5.** Evolution of C-H and C-N peaks for pure and diluted formamide ice samples: the initial stage is represented in black, and two steps of irradiation in red and blue. (For interpretation of the references to color in this figure legend, the reader is referred to the web version of this article.)

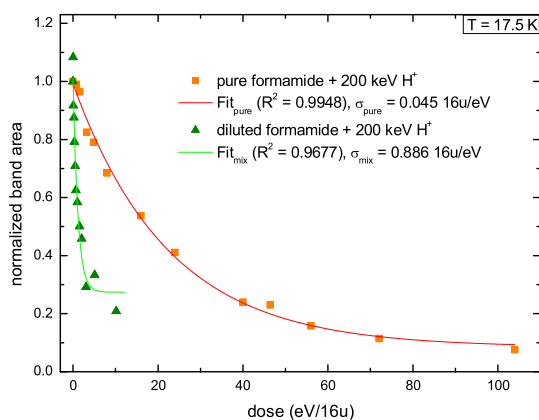


**Fig. 6.** Normalized band area of pure and diluted formamide after ion bombardment plotted vs. irradiation dose. The graph shows data resulting from the irradiation with  $H^+$  200 keV ions and the fit obtained using Eq. (1).

$He^+$ , and  $N^+$ , respectively. For each sample the normalized band area is plotted as a function of the irradiation dose in Fig. 8. Experimental data points are fitted by an exponential curve (Eq. (1)). The destruction cross section values obtained by the fit are reported in Table 1. All the fittings are very good, with coefficients of correlation  $R^2$  around 0.99; the choice of the decreasing exponential fitting is then accurate. It was found that the value of cross section depends on the irradiating ion. Indeed, for 200 keV  $N^+$  a cross section ten times higher than for 200 keV  $H^+$  and three times higher for 200 keV  $He^+$  was found.

### 3.4. Estimation of the radiation dose on the moon

#### 3.4.1. Solar energetic particles and galactic cosmic rays

After the experiments, the OMERE software was utilized to evaluate the effects of GCRs and SEPs on the Moon. A lunar orbit simulation was used to make the assessment. Fig. 9 shows the dose rate as a function of depth calculated by OMERE. The dose is given in units of rad, where  $1 \text{ rad} = 10^{-2} \text{ Gy} = 1.7 \times 10^{-9} \text{ eV/16u}$  (Baratta et al., 2019). The radiation environment on the Moon has been the subject of several investigations. Both simulations and real measurements in situ have been performed (e.g. de Angelis et al., 2008; Schwadron et al., 2012; Crites et al., 2013). In particular, Schwadron et al. (2012) report the dose rate measured at the surface of the Moon by the CRATER instrument on board the Lunar Reconnaissance Orbiter (LRO) mission as well as dose rate values obtained by ACE (Advanced Composition Explorer) spacecraft. The values obtained by OMERE software, shown

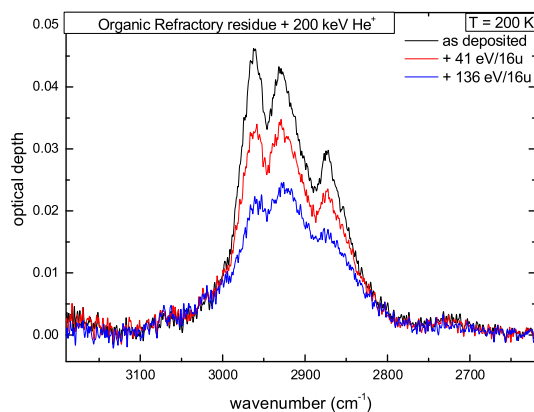


**Fig. 7.** Evolution of C-H stretching mode feature for the organic refractory residue: the initial stage is represented in black, and two steps of irradiation in red and blue. (For interpretation of the references to color in this figure legend, the reader is referred to the web version of this article.)

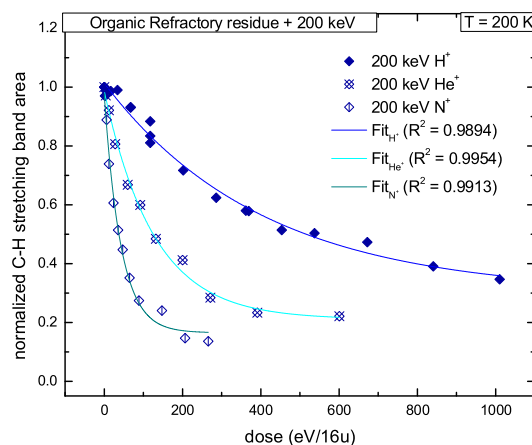


**Fig. 8.** Normalized C-H stretching band area of the organic refractory residue after ion bombardment plotted vs. irradiation dose. The graph shows data obtained from the irradiation with 200 keV  $H^+$ ,  $He^+$  and  $N^+$  and the fit obtained using Eq. (1).

in Fig. 9, are comparable to the values reported by Schwadron et al. (2012) that are in the range of 5–10 Gy/a at the Moon surface. Using the destruction cross section values reported in Table 1 and the dose rate given by OMERE, we have evaluated the lifetime of organic species on the Moon as a function of depth, i.e. the time required for the concentration of a chemical species to decrease to  $1/e$  of its original value. Results are reported in Fig. 10.

#### 3.4.2. Solar wind

In addition to GCRs and SEPs, solar system objects are also exposed to SW, a supersonic flux of ions and electrons released from the solar corona. The ion flux is on the order of  $2 \times 10^8 \text{ ions cm}^{-2} \text{ s}^{-1}$  (Schwenn, 2001) at 1 au (astronomical unit,  $1.495 \times 10^{11} \text{ m}$ ), with an energy of 1 keV per atomic mass unit. The SW ions consist of  $H^+$  (96%) and  $He^{2+}$  (4%), heavier elements having abundances  $<0.1\%$ . The flux decays as  $1/r^2$ , where  $r$  is the distance from the Sun (e.g. Baratta et al., 2004). Since OMERE does not account for particles with energy below 10 keV, we estimate the effects of SW ions by means of SRIM. Table 2 displays SRIM input parameters and outcomes. Calculation were made considering a layer of  $SiO_2$  (thickness = 1000 Å). The different abundance of hydrogen and helium ions was also taken into account. We considered three cross section values among those reported in Table 1, i.e. the smallest ( $\sigma_1 = 0.002 \text{ 16u/eV}$ ), an intermediate one ( $\sigma_2 = 0.045 \text{ 16u/eV}$ ) and the highest ( $\sigma_3 = 0.886 \text{ 16u/eV}$ ) to estimate the lifetime of organic

**Table 2**

SRIM calculation parameters and results. The input layer thickness is 1000 Å for each measurement. The lifetime under SW irradiation has been estimated using the cross sections  $\sigma_1$ ,  $\sigma_2$  and  $\sigma_3$ , which refer respectively to the organic residue,  $\text{NH}_2\text{CHO}$  and  $\text{Ar}:\text{NH}_2\text{CHO}$  mixture.

Layer composition	Density (g cm <sup>-3</sup> )	ion (energy)	Stopping power (eV/Å)	Dose rate (10 <sup>-6</sup> eV/16u s)	Penetration depth (Å)	Lifetime (a <sup>a</sup> )		
						$\sigma_1$	$\sigma_2$	$\sigma_3$
SiO <sub>2</sub>	2.7	H <sup>+</sup> (1 keV)	2.5	0.48	292	67	3.5	0.2
SiO <sub>2</sub>	2.7	He <sup>2+</sup> (4 keV)	4	0.03	573	1000	50	2.3

<sup>a</sup> a is the IUPAC symbol for year.

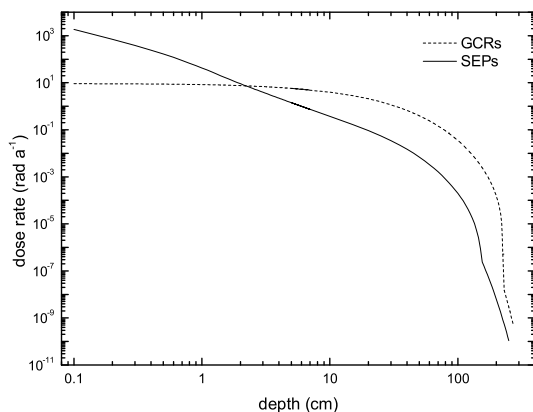


**Fig. 9.** Dose rate vs. depth as calculated by OMERE software (<https://www.trad.fr/spatial/logiciel-omere/>).

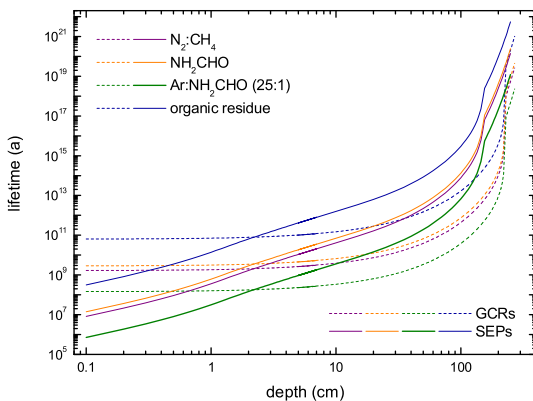


**Fig. 10.** Lifetime on the Moon surface of analyzed organic materials resulting from OMERE simulation of SEPs and GCRs effects vs. depth.

species; the results show that SW ions affect the uppermost 100 nm surface layers and that the lifetime ranges between a fraction of year and 10<sup>3</sup> a.

### 3.5. Estimation of impact gardening effects

Impact gardening is known to affect the surface of airless solar system bodies (e.g. Costello et al., 2020, 2021): this phenomenon stir and mix the outermost crust provoking resurfacing. As a consequence, impact gardening and space weathering processes compete with each other. As shown by Costello et al. (2021), impact gardening is a fast process at the surface while it is slower as depth increases. Taking into account the rate at which gardening proceeds to greater depth with time reported by Costello et al. (2021), we estimated the fraction of surviving organic matter for the Moon as a function of depth over its age.

Given the dose rate  $d(x)$  shown in Fig. 9 and the gardening time  $t_G(x)$  reported in Costello et al. (2021), the dose  $D(x)$  in eV/16u, is

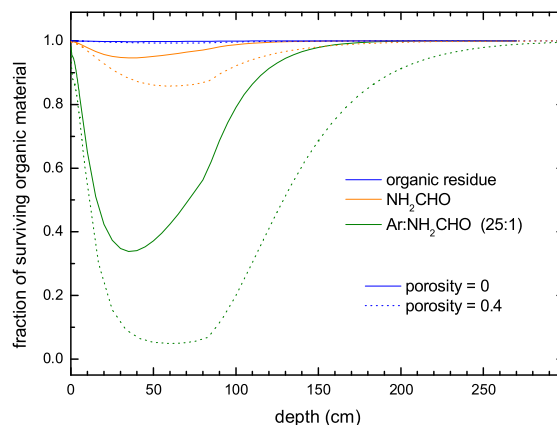


**Fig. 11.** Estimated fraction of surviving organic matter on the Moon as a function of depth. Three different values of destruction cross section and two different values of lunar regolith porosity were used.

given by

$$D(x) = 1.7 \times 10^{-9} \times d(x) \times t_G(x). \quad (2)$$

Then the fraction of surviving organic matter is obtained by

$$y(x) = \frac{N(x)}{N_0} = e^{-\sigma D(x)}, \quad (3)$$

where  $\sigma$  (16u/eV) is the cross section obtained experimentally.

In Fig. 11 the results for three different values of destruction cross section (namely  $\sigma_1 = 0.002$  16u/eV,  $\sigma_2 = 0.045$  16u/eV, and  $\sigma_3 = 0.886$  16u/eV) and for two different values of lunar regolith porosity are reported. As shown by Costello et al. (2021), impact gardening is a fast process at the surface while it is slower as depth increases. This means that at the surface the material is irradiated (space weathering) for a short time and a significant fraction of organic matter, if present, would survive. As we move inward, the gardening process is slower and the material is irradiated for longer time; this means that the fraction of organic matter that survives is smaller. As depth increases further the gardening process is even slower and in principle organic matter could be irradiated for longer time however at greater depth the dose rate decreases significantly (see Fig. 9) and as a consequence the fraction of present organic matter that survive is high. Porosity is a measure of voids in the regolith matter. The dose rate values reported in Fig. 9 refer to a compact solid. If voids were present, the dose rate at a given depth would be higher. In turns this means that at a given depth space weathering effects would be higher and the surviving fraction of organic material would be smaller.

## 4. Discussion

We obtained the destruction cross section under ion irradiation of compounds that simulate organics at the Moon's surface. Our work extends previous investigations on the survival of organic substances irradiated by fast ions (e.g. Gerakines et al., 2012; Gerakines and Hudson, 2013; Urso et al., 2022) and UV photons (e.g. Fornaro et al.,

2018; Baratta et al., 2019; Corazzi et al., 2020; Suhasaria and Menella, 2022). We found that (1) for a given species (e.g.  $\text{NH}_2\text{CHO}$ ) the destruction cross section depends on the matrix it is embedded in with; in fact, if  $\text{NH}_2\text{CHO}$  is highly diluted in an inert matrix, the destruction cross section is more than one order of magnitude higher than the value obtained in the case of pure  $\text{NH}_2\text{CHO}$ ; This result has already been reported in the case of ion irradiation of pure  $\text{H}_2\text{O}$  ice and  $\text{H}_2\text{O}$ -rich ice mixtures (e.g. Gomis et al., 2004; Garozzo et al., 2011) and  $\text{H}_2\text{O}$  trapped in a matrix (Fulvio et al., 2010). In fact when energetic ions travel through the target the energy they release causes the break of chemical bonds which in turn causes the formation of radicals and fragments. These radicals and fragments might react to each other and form molecular species not originally present in the target. In the case of a target made of a single molecular species the probability of chemical reactions which re-form the original species (backward reactions) is very high. When a given molecular species is highly diluted in a matrix the probability of backward reactions is very low and the species is rapidly destroyed. (2) in the case of the organic refractory residue, the destruction cross section is more than one order of magnitude lower than the value obtained for volatile species. Furthermore, we used different ions at 200 keV energy (namely  $\text{H}^+$ ,  $\text{He}^+$ , and  $\text{N}^+$ ) and we found that the destruction cross section value for an ice mixture is independent of the projectile (see Table 1). This result is in agreement with the recent work by De Sanctis et al. (2023): they found the same value of destruction cross section after ion irradiation of an aliphatic organic compound (undecanoic acid,  $\text{C}_{10}\text{H}_{21}\text{COOH}$ ) mixed with minerals.

The organic refractory residue is a carbon-rich material with several functional groups embedded in a complex structure (e.g. Palumbo et al., 2004; Accolla et al., 2018; Urso et al., 2020). The destruction cross section value of residues exposed to ion bombardment varies by nearly an order of magnitude when different projectiles are taken into account (see Table 1). This is the first time that such a result is reported for organic refractory residues. The comprehension of the physico-chemical mechanisms which give this result is beyond the scope of this work. We are planning further experiments to shed light on the processes at the origin of the differences we observed. Furthermore, we plan to perform new experiments considering different organic refractory residues and other refractory organic compounds to verify the generality of this result.

Energetic charged particles of all energies can strike the lunar surface since there is neither a magnetic shield nor an atmosphere. We estimated the dose rate due to GCRs and SEPs at the Moon (see Fig. 9) and, with the cross section values measured experimentally, we obtained the expected lifetime of organic compounds on the surface of the Moon (see Fig. 10). As shown in Figs. 9 and 10, SEPs and GCRs effects prevail over each other based on depth; in the uppermost layers the action of SEPs is dominant, while below about 2 cm from the surface, the dose rate and hence the lifetime of organic compounds depend on GCRs. Moreover, running SRIM software we estimated the lifetime considering the contribution by SW ions that is relevant in the topmost 100 nm of the surface (see Table 2).

In Fig. 11 we plot the fraction of surviving organic material assuming the impact gardening model by Costello et al. (2021) and the dose rate and destruction cross section presented in this work. The trend shown in Fig. 11 describes the expected fraction of surviving organic materials in those regions exposed to energetic radiation (i.e. both SEPs and GCRs effects are present).

The description of the fate of organic species in permanently shadowed regions (PSRs) at the lunar poles is not straightforward. In fact, in those regions the evolution of volatile species is driven also by diffusion and sublimation. These regions are characterized by low surface temperatures ( $T < 100$  K), which allow the presence of water ice (e.g. Watson et al., 1961; Gläser et al., 2021). Other volatile species are expected to be trapped in it and, indeed, have been detected in the LCROSS ejecta plume (Colaprete et al., 2010) and by the observations

obtained with the Nighttime Lyman Alpha Mapping Project (LAMP) UV spectrograph onboard the LRO (Magaña et al., 2023). However, the presence of super volatile species (such as  $\text{CH}_4$ ,  $\text{N}_2$ , and  $\text{CO}$ ) requires temperature values as low as 20–30 K (e.g. O'Brien and Byrne, 2022, and references therein). Laboratory experiments have shown that, at temperatures lower than the sublimation temperature, volatile species such as  $\text{CH}_4$ ,  $\text{N}_2$ , and  $\text{CO}$  diffuse in water ice (Palumbo, 2006; Raut et al., 2007; Fulvio et al., 2010). It is expected that molecules that diffuse toward the surface would rapidly sublimate while molecules that diffuse inward would remain trapped in cold icy layers. This is consistent with the detection of  $\text{CH}_4$  in the LCROSS ejecta plume originating from layers deeper than about 0.7 m (Colaprete et al., 2010). Less volatile species, such as  $\text{NH}_2\text{CHO}$ , and the organic refractory residue are not expected to be affected by diffusion and sublimation. In permanently shadowed regions the flux of energetic ions is expected to be lower than the flux on regions fully exposed to solar radiation. As a consequence also the dose rate is expected to be lower while the impact gardening is not expected to vary significantly with solar irradiation. Then the fraction of surviving material reported in Fig. 11 would be underestimated because it has been obtained considering both SEPs and GCRs effects. As a consequence, the values of the surviving fraction reported in Fig. 11 can be regarded as a lower limit. Finally, the fraction of surviving organic refractory residue is close to 1 even in regions exposed to solar radiation.

C-rich materials were detected on the surface of black pyroclastic beads collected in the Shorty crater during the Apollo 17 mission. Thomas-Keprta et al. (2014) explained their presence considering the delivery of exogenous C-rich matter from micrometeorite impacts. This C-rich material is on average more disordered than the C-rich material in IDPs collected on Earth. Our experiments show that the exposure of organic residues to 200 keV ions causes the destruction of the C-H bonds with increasing the dose. Previous experiments (Strazzulla and Baratta, 1992; Ferini et al., 2004; Palumbo et al., 2004; Urso et al., 2020) showed that increasing irradiation dose causes the loss of the H content of organic materials and their progressive conversion into amorphous carbon. Such material presents a featureless IR spectrum but shows characteristic bands in Raman spectra (G and D lines at 1560 and 1360  $\text{cm}^{-1}$ , respectively). As discussed above, organic refractory residues obtained after ion irradiation of simple ices can be considered analogues of organic matter in space. Indeed they are good spectral analogues of extraterrestrial organic material detected in micrometeorites and interplanetary dust particles (IDPs) (Baratta et al., 2015; Potapov et al., 2022).

These results are compatible with the hypothesis that refractory carbonaceous matter detected on the Moon has an exogenous origin and its high disorder level is a consequence of the exposure to energetic radiation.

#### CRediT authorship contribution statement

**G.L. Dalla Pria:** Data curation, Formal analysis, Investigation, Writing – original draft. **O. Sohier:** Data curation, Formal analysis, Writing – review & editing. **C. Scirè:** Investigation, Visualization, Writing – review & editing. **R.G. Urso:** Formal analysis, Writing – review & editing, Conceptualization. **G.A. Baratta:** Conceptualization, Formal analysis, Investigation, Writing – review & editing. **M.E. Palumbo:** Supervision, Methodology, Investigation, Funding acquisition, Data curation, Conceptualization, Validation, Writing – original draft.

#### Declaration of competing interest

The authors declare that they have no known competing financial interests or personal relationships that could have appeared to influence the work reported in this paper.

## Data availability

Data will be made available on request.

## Acknowledgments

This work has been supported by the project PRIN-INAF 2016 The Cradle of Life - GENESIS-SKA (General Conditions in Early Planetary Systems for the rise of life with SKA) and by the Italian Ministero dell'Istruzione, dell'Università e della Ricerca through the grant Progetti Premiali 2012-iALMA (CUP C52I13000140001). The authors are grateful to S. Pirrotta, Th. Orlando and the team at the Center for Lunar Environment and Volatile Exploration Research (CLEVER) for stimulating and fruitful discussions.

## References

- Accolla, M., Pellegrino, G., Baratta, G.A., Condorelli, G.G., Fedoseev, G., Scirè, C., Palumbo, M.E., Strazzulla, G., 2018. Combined IR and XPS characterization of organic refractory residues obtained by ion irradiation of simple icy mixtures. *Astron. Astrophys.* 620, A123. <http://dx.doi.org/10.1051/0004-6361/201834057>.
- Baratta, G.A., Accolla, M., Chaput, D., Cottin, H., Palumbo, M.E., Strazzulla, G., 2019. Photolysis of cometary organic dust analogs on the EXPOSE-R2 mission at the international space station. *Astrobiology* 19, 1018–1036. <http://dx.doi.org/10.1089/ast.2018.1853>.
- Baratta, G.A., Chaput, D., Cottin, H., Fernandez Cascales, L., Palumbo, M.E., Strazzulla, G., 2015. Organic samples produced by ion bombardment of ices for the EXPOSE-R2 mission on the international space station. *Planet. Space Sci.* 118, 211–220. <http://dx.doi.org/10.1016/j.pss.2015.08.011>.
- Baratta, G.A., Mennella, V., Brucato, J.R., Colangeli, L., Leto, G., Palumbo, M.E., Strazzulla, G., 2004. Raman spectroscopy of ion-irradiated interplanetary carbon dust analogues. *J. Raman Spectrosc.* 35, 487–496. <http://dx.doi.org/10.1002/jrs.1169>.
- Barucci, M.A., Merlin, F., 2020. Surface Composition of Trans-Neptunian Objects. Elsevier, pp. 109–126. <http://dx.doi.org/10.1016/B978-0-12-816490-7.00005-9>.
- Bockelée-Morvan, D., Lis, D.C., Wink, J.E., Despois, D., Crovisier, J., Bachiller, R., Benford, D.J., Biver, N., Colom, P., Davies, J.K., Gérard, E., Germain, B., Houde, M., Mehlinger, D., Moreno, R., Paubert, G., Phillips, T.G., Rauer, H., 2000. New molecules found in comet C/1995 O1 (Hale-Bopp). Investigating the link between cometary and interstellar material. *Astron. Astrophys.* 353, 1101–1114.
- Boogert, A.C.A., Gerakines, P.A., Whittet, D.C.B., 2015. Observations of the icy universe. *Annu. Rev. Astron. Astrophys.* 53, 541–581. <http://dx.doi.org/10.1146/annurev-astro-082214-122348>.
- Brucato, J.R., Baratta, G.A., Strazzulla, G., 2006. An infrared study of pure and ion irradiated frozen formamide. *Astron. Astrophys.* 455, 395–399. <http://dx.doi.org/10.1051/0004-6361:20065095>.
- Clendenen, A.R., Aleksandrov, A., Jones, B.M., Loutzenhisser, P.G., Britt, D.T., Orlando, T.M., 2022. Temperature programmed desorption comparison of lunar regolith to lunar regolith simulants LMS-1 and LHS-1. *Earth Planet. Sci. Lett.* 592, 117632. <http://dx.doi.org/10.1016/j.epsl.2022.117632>.
- Colaprete, A., Schultz, P., Heldmann, J., Wooden, D., Shirley, M., Ennico, K., Hermany, B., Marshall, W., Ricco, A., Elphic, R.C., Goldstein, D., Summy, D., Bart, G.D., Asphaug, E., Korycansky, D., Landis, D., Sollitt, L., 2010. Detection of water in the LCROSS ejecta plume. *Science* 330, 463–468. <http://dx.doi.org/10.1126/science.1186986>.
- Collings, M.P., Anderson, M.A., Chen, R., Dever, J.W., Viti, S., Williams, D.A., McCoustra, M.R.S., 2004. A laboratory survey of the thermal desorption of astrophysically relevant molecules. *Mon. Not. R. Astron. Soc.* 354, 1133–1140. <http://dx.doi.org/10.1111/j.1365-2966.2004.08272.x>.
- Corazzi, M.A., Fedele, D., Poggiali, G., Brucato, J.R., 2020. Photoprocessing of formamide ice: route towards prebiotic chemistry in space. *Astron. Astrophys.* 636, A63. <http://dx.doi.org/10.1051/0004-6361/202037587>.
- Costello, E.S., Ghent, R.R., Hirabayashi, M., Lucey, P.G., 2020. Impact gardening as a constraint on the age, source, and evolution of ice on Mercury and the moon. *J. Geophys. Res.: Planets* 125, 3. <http://dx.doi.org/10.1029/2019JE006172>.
- Costello, E.S., Ghent, R.R., Lucey, P.G., 2021. Secondary impact burial and excavation gardening on the moon and the depth to ice in permanent shadow. *J. Geophys. Res.: Planets* 126, 9. <http://dx.doi.org/10.1029/2021JE006933>.
- Crites, S.T., Lucey, P.G., Lawrence, D., 2013. Proton flux and radiation dose from galactic cosmic rays in the lunar regolith and implications for organic synthesis at the poles of the Moon and Mercury. *Icarus* 226, 1192–1200. <http://dx.doi.org/10.1016/j.icarus.2013.08.003>.
- Cruikshank, D.P., Schmitt, B., Roush, T.L., Owen, T.C., Quirico, E., Geballe, T.R., de Bergh, C., Bartholomew, M.J., Dalle Ore, C.M., Douté, S., Meier, R., 2000. Water ice on Triton. *Icarus* 147, 309–316. <http://dx.doi.org/10.1006/icar.2000.6451>.
- Danger, G., Orthous-Daunay, F.R., de Marcellus, P., Modica, P., Vuitton, V., Duverney, F., Flandinet, L., Le Sergeant d'Hendecourt, L., Thissen, R., Chiavassa, T., 2013. Characterization of laboratory analogs of interstellar/cometary organic residues using very high resolution mass spectrometry. *Geochim. Cosmochim. Acta* 118, 184–201. <http://dx.doi.org/10.1016/j.gca.2013.05.015>.
- de Angelis, G., Badavi, F.F., Clem, J.M., Blattning, S.R., Cloudsley, M.S., Tripathi, R.K., Wilson, J.W., 2008. Modeling of the radiation environment on the Moon. In: Bhardwaj, A. (Ed.), *Advances in Geosciences*. Vol. 19, Planetary Science, [http://dx.doi.org/10.1142/9789812838162\\_0008](http://dx.doi.org/10.1142/9789812838162_0008).
- De Sanctis, M.C., Baratta, G.A., Brucato, J.R., De Angelis, S., Ferrari, M., Fulvio, D., Germanà, M., Mennella, V., Palumbo, M.E., Pagnoscini, S., Poggiali, G., Popa, C., Scirè, C., Strazzulla, G., 2023. Degradation of organic matter on Ceres: results from laboratory experiments on irradiated samples. In: *54th Lunar and Planetary Science Conference*. Vol. 118, pp. 184–201.
- Ferini, G., Baratta, G.A., Palumbo, M.E., 2004. A Raman study of ion irradiated icy mixtures. *Astron. Astrophys.* 414, 757. <http://dx.doi.org/10.1051/0004-6361:20031641>.
- Fornaro, T., Boosman, A., Brucato, J.R., ten Kate, L.L., Siljeström, S., Poggiali, G., Steele, A., Hazen, R.M., 2018. UV irradiation of biomarkers adsorbed on minerals under Martian-like conditions: Hints for life detection on Mars. *Icarus* 313, 38–60. <http://dx.doi.org/10.1016/j.icarus.2018.05.001>.
- Fulvio, D., Guglielmino, S., Favone, T., Palumbo, M.E., 2010. Near-infrared laboratory spectra of H<sub>2</sub>O trapped in N<sub>2</sub>, CH<sub>4</sub>, and CO: hints for trans-Neptunian objects' observations. *Astron. Astrophys.* 511, A62. <http://dx.doi.org/10.1051/0004-6361/200912893>.
- Garozzo, M., La Rosa, L., Kaňuchová, Z., Ioppolo, S., Baratta, G.A., Palumbo, M.E., Strazzulla, G., 2011. The influence of temperature on the synthesis of molecules on icy grain mantles in dense molecular clouds. *Astron. Astrophys.* 528, A118. <http://dx.doi.org/10.1051/0004-6361/201015341>.
- Gerakines, P.A., Hudson, R.L., 2013. Glycine's radiolytic destruction in ices: first in situ laboratory measurements for Mars. *Astrobiology* 13, 7. <http://dx.doi.org/10.1089/ast.2012.0943>.
- Gerakines, P.A., Hudson, R.L., Moore, M.H., Bell, J.-L., 2012. In situ measurements of the radiation stability of amino acids at 15–140 K. *Icarus* 220, 647–659. <http://dx.doi.org/10.1016/j.icarus.2012.06.001>.
- Gläser, P., Sanin, A., Williams, J.-P., Mitrofanov, I., Oberst, J., 2021. Temperatures near the lunar poles and their correlation with hydrogen predicted by LEND. *J. Geophys. Res.: Planets* 126, 9. <http://dx.doi.org/10.1029/2020JE006598>.
- Glotch, T., Schmidt, G., Pendleton, Y., 2019. Introduction to science and exploration of the moon, near-earth asteroids, and moons of mars. *J. Geophys. Res.: Planets* 124, 1635–1638. <http://dx.doi.org/10.1029/2019JE005961>.
- Goesmann, F., Rosenbauer, H., Bredehöft, J.H., Cabane, M., Ehrenfreund, P., Gautier, T., Giri, C., Krüger, H., Le Roy, L., MacDermott, A.J., McKenna-Lawlor, S., Meierhenrich, U., Caro, G., Raulin, F., Roll, R., Steele, A., Steininger, H., Sternberg, R., Szopa, C., Ulamec, S., 2015. Organic compounds on comet 67P/Churyumov-Gerasimenko revealed by COSAC mass spectrometry. *Science* 349, <http://dx.doi.org/10.1126/science.aab0689>.
- Gomis, O., Leto, G., Strazzulla, G., 2004. Hydrogen peroxide production by ion irradiation of thin water ice films. *Astron. Astrophys.* 420, 405–410. <http://dx.doi.org/10.1051/0004-6361:20041091>.
- Grundy, W.M., Buie, M.W., 2001. Distribution and evolution of CH<sub>4</sub>, N<sub>2</sub>, and CO ices on Pluto's surface: 1995 to 1998. *Icarus* 153, 248–263. <http://dx.doi.org/10.1006/icar.2001.6684>.
- Johnson, R.E., 1990. *Energetic Charged-Particle Interactions with Atmospheres and Surfaces*. Springer Berlin Heidelberg, <http://dx.doi.org/10.1007/978-3-642-48375-2>, 1990.
- Jones, B.M., Aleksandrov, A., Dyar, M.D., Hibbitts, C.A., Orlando, T.M., 2020. Investigation of water interactions with apollo lunar regolith grains. *J. Geophys. Res.: Planets* 125, e2019JE006147. <http://dx.doi.org/10.1029/2019JE006147>.
- Jones, B.M., Aleksandrov, A., Hibbitts, C.A., Orlando, T.M., 2021. Thermal evolution of water and hydrogen from apollo lunar regolith grains. *Earth Planet. Sci. Lett.* 571, 117107. <http://dx.doi.org/10.1016/j.epsl.2021.117107>.
- Loeffler, M.J., Baratta, G.A., Palumbo, M.E., Strazzulla, G., Baragiola, R.A., 2005. CO synthesis in solid CO by lyman- $\alpha$  photons and 200 keV protons. *Astron. Astrophys.* 435, 587–594. <http://dx.doi.org/10.1051/0004-6361:20042256>.
- Magaña, L.O., Retherford, K.D., Byron, B.D., Hendrix, A.R., Grava, C., Mandt, K.E., Raut, U., Czajka, E., Hayne, P.O., Hurley, D.M., Gladstone, G.R., Poston, M.J., Greathouse, T.K., Pryor, W., Cahill, J.T., Stickle, A., 2023. LRO-LAMP lunar south pole cold traps: Assessment of H<sub>2</sub>O and potential CO<sub>2</sub> and NH<sub>3</sub> reserves. *J. Geophys. Res.: Planets* 128, <http://dx.doi.org/10.1029/2023JE007863>.
- Materese, C.K., Nuevo, M., Sandford, S.A., 2017. The formation of nucleobases from the ultraviolet photoirradiation of purine in simple astrophysical ice analogues. *Astrobiology* 17, 761–770. <http://dx.doi.org/10.1089/ast.2016.1613>.
- McLain, J.L., Loeffler, M.J., Farrell, W.M., Honniball, C.I., Keller, J.W., Hudson, R., 2021. Hydroxylation of Apollo 17 soil sample 78421 by solar wind protons. *J. Geophys. Res.: Planets* 126, e2021JE006845. <http://dx.doi.org/10.1029/2021JE006845>.
- Meinert, C., Myrgorodska, I., de Marcellus, P., Buhse, T., Nahon, L., Hoffmann, S.V., d'Hendecourt, L.L.S., Meierhenrich, U.J., 2016. Ribose and related sugars from ultraviolet irradiation of interstellar ice analogs. *Science* 352, 6282. <http://dx.doi.org/10.1126/science.aad8137>.

- Nuevo, M., Cooper, G., Sandford, S.A., 2018. Deoxyribose and deoxysugar derivatives from photoprocessed astrophysical ice analogues and comparison to meteorites. *Nature Commun.* 9, 5276. <http://dx.doi.org/10.1038/s41467-018-07693-x>.
- O'Brien, P., Byrne, S., 2022. Shadows at the lunar poles. *Planet. Sci. J.* 3, 258. <http://dx.doi.org/10.3847/PSJ/ac9e5b>.
- Palumbo, M.E., 2006. Formation of compact solid water after ion irradiation at 15 K. *Astron. Astrophys.* 453, 903–909. <http://dx.doi.org/10.1051/0004-6361/20042382>.
- Palumbo, M.E., Ferini, G., Baratta, G.A., 2004. Infrared and Raman spectroscopies of refractory residues left over after ion irradiation of nitrogen-bearing icy mixtures. *Adv. Space Res.* 33, 49–56. <http://dx.doi.org/10.1016/j.asr.2003.03.002>.
- Pino, S., Sponer, J.E., Costanzo, G., Saladino, R., Mauro, E.D., 2015. From formamide to RNA, the path is tenuous but continuous. *Life* 5, 372–384. <http://dx.doi.org/10.3390/life5010372>.
- Potapov, A., Palumbo, M.E., Dionnet, Z., Longobardo, A., Jäger, C., Baratta, G.A., Rotundi, A., Henning, T., 2022. Exploring refractory organics in extraterrestrial particles. *Astrophys. J.* 935, 158. <http://dx.doi.org/10.3847/1538-4357/ac7f32>.
- Raunier, S., Chiavassa, T., Duvernay, F., Borget, F., Aycard, J.P., Dartois, E., d'Hendecourt, L., 2004. Tentative identification of urea and formamide in ISO-SWS infrared spectra of interstellar ices. *Astron. Astrophys.* 416, 165–169. <http://dx.doi.org/10.1051/0004-6361/20034558>.
- Raut, U., Teolis, B.D., Loeffler, M.J., Vidal, R.A., Famá, M., Baragiola, R.A., 2007. Compaction of microporous amorphous solid water by ion irradiation. *J. Chem. Phys.* 126, 244511. <http://dx.doi.org/10.1051/0004-6361/20034558>.
- Rothard, H., Domaracka, A., Boduch, P., Palumbo, M.E., Strazzulla, G., da Silveira, E.F., Dartois, E., 2017. Modification of ices by cosmic rays and solar wind. *J. Phys. B: At. Mol. Opt. Phys.* 50, 6. <http://dx.doi.org/10.1088/1361-6455/50/6/062001>.
- Saladino, R., Crestini, C., Ciceriello, F., Pino, S., Costanzo, G., Di Mauro, E., 2009. From formamide to RNA: the roles of formamide and water in the evolution of chemical information. *Res. Microbiol.* 160, 441–448. <http://dx.doi.org/10.1016/j.resmic.2009.06.001>.
- Saladino, R., Crestini, C., Neri, V., Brucato, J.R., Colangeli, L., Ciceriello, F., Di Mauro, E., Costanzo, G., 2005. Synthesis and degradation of nucleic Acid components by formamide and cosmic dust analogues. *Chembiochem* 6, 1368–1374. <http://dx.doi.org/10.1002/cbic.200500035>.
- Saladino, R., Crestini, C., Pino, S., Costanzo, G., Di Mauro, E., 2012. Formamide and the origin of life. *Phys. Life Rev.* 9, 84–104. <http://dx.doi.org/10.1016/j.plrev.2011.12.002>.
- Schutte, W.A., Boogert, A.C.A., Tielens, A.G.G.M., Whittet, D.C.B., Gerakines, P.A., Chiar, J.E., Ehrenfreund, P., Greenberg, J.M., van Dishoeck, E.F., de Graauw, T., 1999. Weak ice absorption features at 7.24 and 7.41  $\mu\text{m}$  in the spectrum of the obscured young stellar object W 33A. *Astron. Astrophys.* 343, 966–976.
- Schwadron, N.A., Baker, T., Blake, B., Case, A.W., Cooper, J.F., Golightly, M., Jordan, A., Joyce, C., Kasper, J., Kozarev, K., Mislinski, J., Mazur, J., Posner, A., Rother, O., Smith, S., Spence, H.E., Townsend, L.W., Wilson, J., Zeitlin, C., 2012. Lunar radiation environment and space weathering from the cosmic ray telescope for the effects of radiation (CRaTER). *J. Geophys. Res.: Planets* 117, E12. <http://dx.doi.org/10.1029/2011JE003978>.
- Schwenn, R., 2001. *Encyclopedia of Astronomy & Astrophysics, Solar Wind: Global Properties*. IOP Publishing Ltd, <http://dx.doi.org/10.1201/9781003220435>, 2005.
- Scirè, C., 2017. Guide for the Tool “ICE Thickness Calculator”. Technical Report INAF LAsP 1/2017, URL: <https://openaccess.inaf.it/handle/20.500.12386/818>.
- Scirè, C., Urso, R.G., Fulvio, D., Baratta, G.A., Palumbo, M.E., 2019. Mid-IR band strength, density, refractive index, and thermal evolution study for solid CH<sub>2</sub>DOH pure and in astrophysical relevant mixtures. *Spectrochim. Acta A* 219, 288–296. <http://dx.doi.org/10.1016/j.saa.2019.04.021>.
- Seperuelo Duarte, E., Domaracka, A., Boduch, P., Rothard, H., Dartois, E., da Silveira, E.F., 2010. Laboratory simulation of heavy-ion cosmic-ray interaction with condensed CO. *Astron. Astrophys.* 512, A71. <http://dx.doi.org/10.1051/0004-6361/200912899>.
- Strazzulla, G., Baratta, G.A., 1992. Carbonaceous material by ion irradiation in space. *Astron. Astrophys.* 266, 434–438.
- Suhasaria, T., Mennella, V., 2022. Ly $\alpha$  irradiation of solid-state formamide. *Astron. Astrophys.* 662, A73. <http://dx.doi.org/10.1051/0004-6361/202243431>.
- Thomas-Keptra, K.L., Clemett, S.J., Messenger, S., Ross, D.K., Le, L., Rahman, Z., McKay, D.S., Gibson, E.K., Gonzalez, C., Peabody, W., 2014. Organic matter on the Earth's Moon. *Geochim. Cosmochim. Acta* 134, 1–15. <http://dx.doi.org/10.1016/j.gca.2014.02.047>.
- Urso, R.G., Hénault, E., Brunetto, R., Baklouti, D., Baratta, G.A., Djouadi, Z., El-saesser, A., Scirè, C., Strazzulla, G., Palumbo, M.E., 2022. Ion irradiation triggers the formation of the precursors of complex organics in space. *Astron. Astrophys.* 668, A169. <http://dx.doi.org/10.1051/0004-6361/202244522>.
- Urso, R.G., Scirè, C., Baratta, G.A., Brucato, J.R., Compagnini, G., Kaňuchová, Z., Palumbo, M.E., Strazzulla, G., 2017. Infrared study on the thermal evolution of solid state formamide. *Phys. Chem. Chem. Phys.* 19, 21759. <http://dx.doi.org/10.1039/C7CP03959J>.
- Urso, R.G., Scirè, C., Baratta, G.A., Compagnini, G., Palumbo, M.E., 2016. Combined infrared and Raman study of solid CO. *Astron. Astrophys.* 594, A80. <http://dx.doi.org/10.1051/0004-6361/201629030>.
- Urso, R.G., Vuitton, V., Danger, G., Le Sergeant d'Hendecourt, L., Flandinet, L., Djouadi, Z., Mivumbi, O., Orthous-Daunay, F.R., Ruf, A., Vinogradoff, V., Wolters, C., Brunetto, R., 2020. Irradiation dose affects the composition of organic refractory materials in space. *Astron. Astrophys.* 644, A115. <http://dx.doi.org/10.1051/0004-6361/202039528>.
- Watson, K., Murray, B.C., Brown, H., 1961. The behavior of volatiles on the lunar surface. *J. Geophys. Res.* 66, 1598. <http://dx.doi.org/10.1029/JZ066i009p03033>.
- Ziegler, J.F., 1977. *The Stopping and Range of Ions in Matter, V. 2–6*. Pergamon Press.
- Ziegler, J.F., Biersack, J.P., Littmark, U., 1996. *The Stopping and Range of Ions in Solids*. Pergamon Press.